International Journal of Systems Science

ISSN: 0020-7721 (Print) 1464-5319 (Online) Journal homepage: https://www.tandfonline.com/loi/tsys20

Path following with a security margin for mobile robots

T. Hamel , P. SouÈres & D. Meizel

To cite this article: T. Hamel , P. SouÈres & D. Meizel (2001) Path following with a security margin for mobile robots, International Journal of Systems Science, 32:8, 989-1002

To link to this article: https://doi.org/10.1080/00207720117537

Published online: 26 Nov 2010.

International Journal of Systems Science, 2001, volume 32, number 8, pages 989–1002

Path following with a security margin for mobile robots

T. Hamel†, P. Souères‡ and D. Meizel§

This paper addresses the problem of determining a feedback control law, robust with respect to localization errors, allowing a mobile robot to follow a prescribed path. The model that we consider is a dynamic extension of the usual kinematic model of a mobile robot in the sense that the path curvature is defined as a new state variable. The control variables are the linear velocity and the derivative of the curvature. By defining a sliding manifold we determine a stabilizing controller for the nominal system, that is when the exact configuration is supposed to be known. Then, we prove that the system remains stable when the feedback control inputs use estimated values instead of the exact values, and we characterize the control robustness with respect to localization and curvature estimation errors. The control robustness is expressed by determining a bounded attractive domain containing the configuration error as the closed-loop control is performed with the estimated state values. Two control laws are successively proposed. The former is deduced from Lyapunov's direct method, and the latter is based on variable structure control techniques. Using variable structure control we show that the size of the attractive domain can be easily minimized while keeping the balance between short response time, low output oscillation, and large stability domain. Knowledge of this attractive domain allows us to compute easily a security margin to guarantee obstacle avoidance during the path following process. Experimental results are presented at the end of the paper.

1. Introduction

One difficult question inherently linked to mobile robots' autonomy is the design of feedback control laws allowing stabilization of their motion. The main difficulty of the problem comes from the non-holonomic rolling without slipping constraint of the wheels on the floor which reduces the set of instantaneous velocities at each time. This navigation problem has motivated a large number of research studies for the past 10 years. The problem is commonly divided into three subproblems, which are path following, trajectory tracking and point stabilization (see for instance Canudas *et al.* (1994) and DeLuca *et al.* (1997) for a survey). As the central problem is stated in terms of designing closed-loop controllers taking into account the kinematic non-holonomic rolling without slipping constraint, few research studies have tried to integrate the vehicle's dynamics in their model. The investigations by Tounsi *et al.* (1995) and Thuilot (1994) constitute a first interesting effort in this direction. Most studies devoted to this problem have considered only kinematic models. Nonlinear feedback controllers have been proposed (Kanayama *et al.* 1991, Samson and Aït-Abderrahim 1991). The main idea behind these algorithms is to define velocity control inputs stabilizing the closed-loop system. However, considering the robot's kinematics only induces a strong limitation in practice. It can be very satisfactory, from a theoretical point of view, to use a static controller assuming that the reference path has a continuous curvature. However, most existing path planners propose paths along which the curvature is only almost everywhere continuous. See for instance the non-holonomic planner presented by Laumond *et al.* (1994) which is based on curves obtained by Reeds and Shepp made up with arcs of circle and line

Received 1 June 1999. Revised 5 September 2000. Accepted 12 September 2000.

† Université d'Evry Val d'Essonnes, CEMIF, 40 rue de Pelvoux, CE 1455, 91000 Courcouronnes, France. email: thamel@iup.univ.evry.fr.

‡ Laboratoire d'Automatique et d'Analyse des Systèmes, CNRS, 7 avenue du Colonel Roche, 31077 Toulouse Cedex 4, France, e-mail: soueres@laas.fr.

§ Université de Technologies de Compiègne–HEUDIASYC, UMR CNRS 6599, BP 20529 60205 Compiègne, France. email: dmeizel@utc.fr.

International Journal of Systems Science ISSN 0020–7721 print/ISSN 1464–5319 online © 2001 Taylor & Francis Ltd
http://www.tandf.co.uk/journals
DOI: 10.1080/00207720010015627

segments (Souères and Laumond 1996). The curvature discontinuity occurring between an arc of circle and a line segment (or two arcs) causes the vehicle to move away from the reference path. This phenomenon can be strongly reduced if the robot's acceleration is controlled instead of its velocity.

Another important hypothesis, implicitly made in those studies, is that the robot's configuration is assumed to be perfectly known at each time. This last assumption is known by roboticians to be very unrealistic. Contrary to manipulators, whose basis remains fixed with respect to the reference frame, and for which the position of the end effector may be directly deduced from the measure of the angles between successive links, a mobile robot may drift during its motion and its exact position cannot be determined from the sole use of dead reckoning techniques. For this reason, exteroceptive measurements *must* be processed to update the vehicle localization in order to limit the estimation error. Estimation of the robot's localization has attracted much interest (Leonard and Durrant-Whyte 1991, Preciado *et al.* 1991, Hamel *et al.* 1993). However, even if the data provided by several sensors are merged, the robot's configuration is obtained with some errors which *cannot* be neglected. Using such methods it is possible to estimate the robot localization inside a bounded confidence domain. However, for a tracking task, the condition that the distance between the reference path (trajectory) and the obstacles is greater than the error on the robot position is not sufficient to guarantee the task feasibility. Some studies have considered the propagation of the estimation errors to design safe open-loop trajectories (see for example Siméon and Alami (1994)). Considering closed-loop control, one needs to quantify the precision of the control regulation with respect to the localization error to ensure the task feasibility.

This paper addresses the problem of determining a feedback control law, robust with respect to localization and curvature estimation errors, allowing a mobile robot to follow a prescribed path. The model that we consider is a dynamic extension of the usual kinematic model of a mobile robot in the sense that we define the curvature as a new state variable. The control variables are the linear velocity and the derivative of the curvature.

By means of sliding mode techniques combined with Lyapunov analysis we determine a stabilizing controller for the system, when the state is supposed to be perfectly known. Then, we prove that the system remains stable when the estimated state values are considered instead of the exact values. The robustness property is then expressed by determining, around each point of the nominal trajectory, a bounded attractive domain containing the configuration error, as the feedback control is performed with the estimated values. From this domain, we show that it is easy to compute a security margin to avoid obstacles as the robot follows the prescribed path. These techniques have been successfully applied to design a robust path following controller for a mobile platform ROBUTER^{TM}; experimental results are presented at the end of the paper.

The paper is organized as follows. The problem is stated in section § 2. First, we describe the vehicle's kinematics, and we state the path following control problem for our model (§§ 2.1 and 2.2). Then we introduce the robustness problem and we model the localization and orientation error (§ 2.3). The controller is described in § 3. The stability is first analysed for the nominal case (§ 3.1). Then the robustness is described by computing the attractive domain (§ 3.2) when estimated values are considered. The controller is first deduced from Lyapunov's direct method. Then introducing a discontinuous term we determine a variable structure control. Finally, an account of experimental results is given in the last section (§ 4).

2. Problem statement

The definition of robustness for tracking control naturally stems from both the statement of the path following control (§ 2.2) and the description of the vehicle kinematics (§ 2.1).

2.1. *Vehicle's kinematics*

The model of a mobile robot is shown in figure 1. The system locomotion is made up of two driving wheels mounted on the same axis, and two rear free wheels.

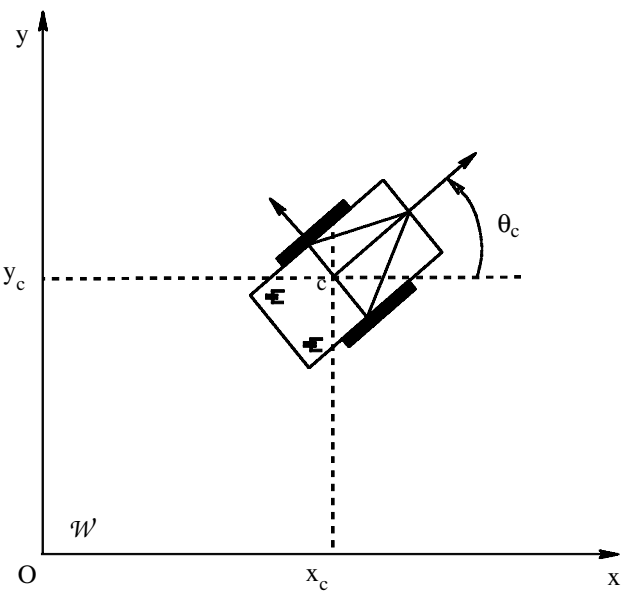

Figure 1. Vehicle configuration.

The motion and orientation are achieved by independent actuators, for example dc motors providing the necessary torques to the driving wheels. Another common model uses a front wheel instead of the two front wheels for driving and steering. Basically both models share the same control and structural properties. The robot configuration with respect to a Cartesian frame $\mathcal{W}\{O, x, y\}$ is completely specified by the vector $P_c = (x_c, y_c, \theta_c)^T$, where (x_c, y_c) are the coordinates of the reference point c and θ_c the orientation of the frame $\mathcal{M}\{c, x_c, y_c\}$ with respect to $\mathcal{W}$ (see figure 1). A simple kinematic model of the oriented point motion is given by:

$$\dot{P}_c(t) = \begin{pmatrix} \dot{x}_c \\ \dot{y}_c \\ \dot{\theta}_c \end{pmatrix} = \begin{pmatrix} v_c \cos\theta_c \\ v_c \sin\theta_c \\ \omega_c \end{pmatrix}, \quad \theta c \in (-\pi, \pi] \qquad (1)$$

where the parameters $(v_c(t), \omega_c(t))^T$ stand for the linear and angular velocities respectively. This model has been considered by numerous workers dealing with non-holonomic control design for wheeled robots. In order to model the actual vehicle dynamics better, we propose here an extension of (1) by controlling the derivative of the realized path curvature instead of the angular velocity. As explained in the introduction, this extension will allow the robot to stay closer to the trajectory when the reference path curvature has isolated discontinuities. The dynamic extension is defined as follows:

$$\begin{pmatrix} \dot{P}_c(t) \\ \dot{\chi}_c(t) \end{pmatrix} = \begin{pmatrix} \dot{x}_c \\ \dot{y}_c \\ \dot{\theta}_c \\ \dot{\chi}_c \end{pmatrix} = \begin{pmatrix} v_c \cos\theta_c \\ v_c \sin\theta_c \\ v_c\chi_c \\ u_c \end{pmatrix}, \qquad (2)$$

where the curvature of the realized trajectory χ_c is viewed as state variable and u_c constitutes an auxiliary input.

2.2. *Path-following control*

Several studies on modelling and control of wheeled robots have been carried out and experimented Nelson and Cox 1988, Sampei *et al.* 1991, Samson 1992, Sordalen 1993). The approach that we have chosen to follow here is that described by Samson (1992), presented in this section as a particular case of the tracking control problem (Hamel and Meizel 1996). The parametrization described by Samson (1992) is defined by means of a Frenet frame $\mathcal{M}'$ whose origin r is the projection of the robot reference point c on the path at each time as shown in figure 2. The path- following problem consists in finding a control law ensuring geometrical convergence towards the reference path regardless of the translational velocity v_c of the robot. Assuming

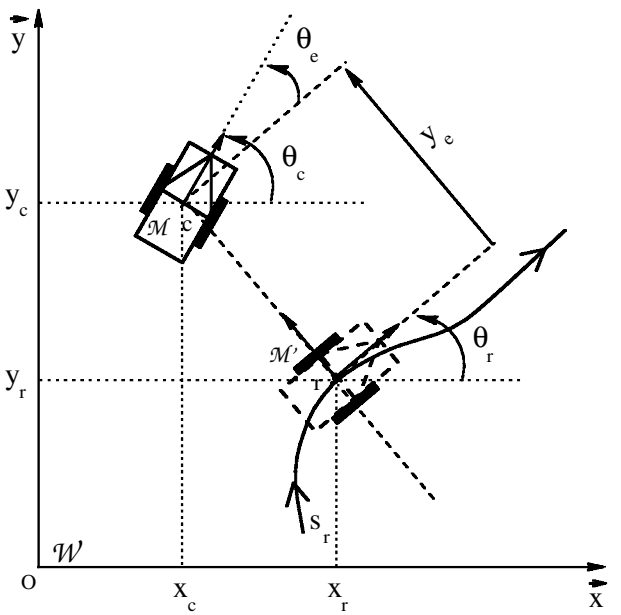

Figure 2. Path following.

that $\mathcal{M}'$ is the frame of a kinematically equivalent fictitious robot, the error configuration vector P_e, with respect to $\mathcal{M}'$, is then

$$P_e = P_e^{\mathcal{M}'} = TP_e^{\mathcal{W}} = T(P_c - P_r), \qquad (3)$$

where $T = \begin{pmatrix} \cos\theta_r & \sin\theta_r & 0 \\ -\sin\theta_r & \cos\theta_r & 0 \\ 0 & 0 & 1 \end{pmatrix}$. The time derivative of the configuration and curvature errors is defined by

$$\begin{pmatrix} \dot{P}_e(t) \\ \dot{\chi}_e(t) \end{pmatrix} = \begin{pmatrix} \dot{x}_e \\ \dot{y}_e \\ \dot{\theta}_e \\ \dot{\chi}_e \end{pmatrix} = \begin{pmatrix} v_c\chi_r^r y_e - v_c\nu_r + v_c\cos\theta_e \\ -v_c\chi_r^r x_e + v_c\sin\theta_e \\ v_c\chi_e \\ u_c - \dot{\chi}_r^r \end{pmatrix}, \qquad (4)$$

where

$$\chi_e = \chi_r^r - \chi_c.$$

χ_r^r is the curvature related to the reference trajectory $(\dot{\theta}_r/v_c)$. ν_r is the relative reference velocity (v_r/v_c).

As the fictitious robot is defined by the orthogonal projection of the robot on the reference path, the first error coordinate x_e and its derivative $\dot{x}_e$ remain equal to zero as the robot moves. Therefore, from the first equation of (4) we have

$$\nu_r = \frac{\cos\theta_e}{1-\chi_r y_e} \tag{5}$$

under the constraint† $(1-\chi_r y_e) > 0$.

From this expression we can define χ_r^r as follows:

$$\chi_r^r = \chi_r \frac{\cos\theta_e}{1-\chi_r y_e}.$$

Introducing the arc length abscissa s_r along the reference path as a new state variable, equations of system (4) can be rewritten as

$$\begin{pmatrix} \dot{s}_r \\ \dot{y}_e \\ \dot{\theta}_e \\ \dot{\chi}_e \end{pmatrix} = \begin{pmatrix} \dfrac{v_c \cos\theta_e}{1-\chi_r y_e} \\ v_c \sin\theta_e \\ v_c\chi_e \\ u_c - \dot{\chi}_r^r \end{pmatrix} \tag{6}$$

The parameters (v_c, u_c) are considered as the vehicle control inputs for the path following process. Regarding (6), the path-following problem may be defined as the search for a control law u_c for steering the triple (y_e, θ_e, χ_e) to $(0,0,0)$. Hence, in the following we consider the reduced system

$$\begin{pmatrix} \dot{y}_e \\ \dot{\theta}_e \\ \dot{\chi}_e \end{pmatrix} = \begin{pmatrix} v_c \sin\theta_e \\ v_c\chi_e \\ u_c - \dot{\chi}_r^r \end{pmatrix}. \tag{7}$$

Remark 1: This representation can also be used when the robot acceleration is controlled instead of its velocity. Considering v_c as a state variable and $\dot{v}_c$ as a new control, the angular acceleration is expressed by

$$\dot{\omega}_c = v_c u_c + \chi_c \dot{v}_c. \tag{8}$$

□

2.3. *Robustness problem*

As stated in the introduction, the current robot configuration as well as the instantaneous path curvature are not exactly measurable. Therefore, the actual inputs of the feedback control are estimated values $(\hat{P}_e^T, \hat{\chi}_e)$ instead of the exact values:

$$u_c = u_c(\hat{P}_e^T, \hat{\chi}_e). \tag{9}$$

Estimates $\hat{P}_e$ of P_e (2) and $\hat{\chi}_e$ of χ_e (4) are obtained from the estimates ($\hat{P}_c = P_c + \delta P_c$ and $\hat{\chi}_c = \chi_c + \delta\chi_c$) of both the configuration and the curvature, continuously updated by combining dead reckoning and exteroceptive measurements (Leonard and Durrant-Whyte 1991, Durieu *et al*. 1996). These estimates belong to a compact confidence domain $(\Omega, \mathcal{X})$ centred around $(\hat{P}_c^T, \hat{\chi}_c)$

† This condition guarantees that the orthogonal projection of the point c on the reference path exists and is unique (see Samson (1992) for details).

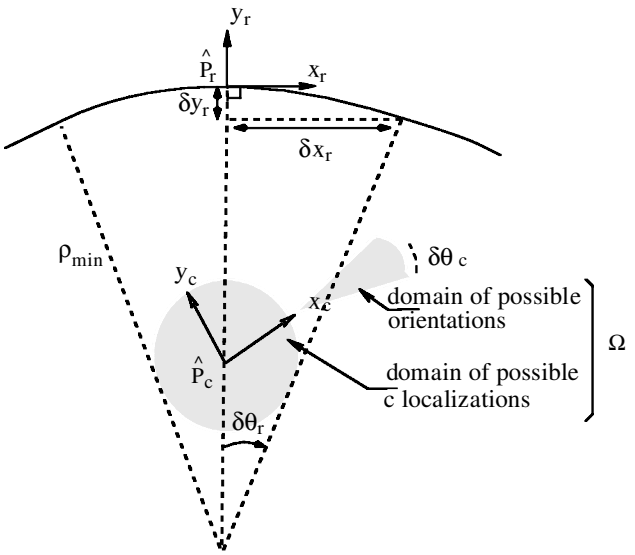

Figure 3. Path following.

(figure 3) $(\hat{P}_c = P_c + \delta P_c; \delta P_c \in \Omega)$. By virtue of extended Kalman filter (EKF) formalism (Cheesman and Smith 1986), or merely for computational ease (Preciado *et al*. 1991), the feasible domain Ω is described as an ellipsoid, a truncated cylinder or a bounding box.

In contrast with the tracking control problem, where errors on the vehicle localization do not modify the target vehicle configuration, it is clear from figure 3 that inaccuracy in the vehicle localization induces an error on the Frenet frame localization with respect to which the variations are defined. Indeed, this frame is obtained by projecting on the nominal curve the set of uncertain† localizations of the characteristic point P_c. If we suppose that $1-\hat{\chi}_r\hat{y}_e > 0$, then $\forall \delta P_c \in \Omega$, an approximated value of δP_r can be deduced geometrically (see figure 3).

$$\begin{pmatrix} \delta x_r \\ \delta y_r \\ \delta\theta_r \end{pmatrix} = \begin{pmatrix} \rho_{min} \sin\delta\theta_r \\ \delta x_r \sin\delta\theta_r \\ \arcsin\left(\dfrac{\delta x_c}{\rho_{min} - y_e}\right) \end{pmatrix}. \tag{10}$$

Taking into account these new inaccuracies, under the assumption that $1-\hat{\chi}_r\hat{y}_e \gg 0$ and $\delta\chi_c \in \mathcal{X} = [-\delta_m\chi_c, \delta_m\chi_c]$ and following (2) we obtain

$$\begin{pmatrix} \hat{P}_e \\ \hat{\chi}_e \end{pmatrix} = \begin{pmatrix} \hat{T}(\hat{P}_c - \hat{P}_r) \\ \hat{\chi}_c - \hat{\chi}_r^r \end{pmatrix} = \begin{pmatrix} P_e + \delta P_e \\ \chi_e + \delta\chi_e \end{pmatrix}, \tag{11}$$

where, from (11) and (12),

† For simplicity, the feasible domain Ω is regarded as a truncated cylinder with flat circular ends containing the domain updated by the EKF.

$$\delta P_e = \begin{pmatrix} \delta x_e \\ \delta y_e \\ \delta \theta_e \end{pmatrix} = \begin{pmatrix} \cos \hat{\theta}_r \delta x_c + \sin \hat{\theta}_r \delta y_c + \delta \theta_r y_e - \delta x_r) \\ -\sin \hat{\theta}_r \delta x_c + \cos \hat{\theta}_r \delta y_c - \delta y_r) \\ \delta \theta_c - \delta \theta_r \end{pmatrix}. \quad (12)$$

In the following, the value of δx_e will be of no importance as the path-following problem only involves the variation in y_e and θ_e. The values of δy_e, $\delta \theta_e$ and $\delta \chi_e$ are not known; however, each of them is supposed to be bounded $|\delta y_e| \leqslant \delta_m y_e$, $|\delta \theta_e| \leqslant \delta_m \theta_e$ and $|\delta \chi_e| \leqslant \delta_m \chi_e$. From the control point of view, the investigated robustness problem can be stated as follows.

Consider the feedback control law (9) with the estimate $(\hat{P}_c^T, \hat{\chi}_c)$ as input instead of the true value (P_c^T, χ_c). Is the equilibrium point of system (4) with the uncertain control law (9) still stable under the assumption that the estimation error $(\delta P_c^T, \delta \chi_c)$ lies in an *a priori* known bounded domain $(\Omega, \mathcal{X})$? Moreover, if the stability is proven, what is the precision of the regulation, that is what is the size of the attractive domain containing $(P_e^T, \chi_e) = 0$?

If the path-following problem can still be achieved when estimated values are considered instead of the exact values, we shall say that the closed-loop controller (9) is robust with respect to localization and curvature estimation errors. More precisely, suppose that we have determined a Lyapunov function $V(P_e^T, \chi_e)$, and a region $\mathcal{S}$ of the (P_e^T, χ_e) space, such that $\forall (P_e^T, \chi_e) \in \mathcal{S}$, $\dot{V}$ is negative definite in the nominal case (i.e. when exact state values are considered). The precision of the regulation domain may be determined by the characterization of a compact domain $\mathcal{A}(\Omega, \mathcal{X}) \subset \mathcal{S}$ such that: $\exists\, \gamma(\Omega, \mathcal{X}) > 0$ such that $\forall (\delta P_c^T, \delta \chi_c) \in \Omega \times \mathcal{X}$, and $\forall (P_e^T, \chi_e) \in \mathcal{S} \setminus \mathcal{A}(\Omega, \mathcal{X})$,

$$V(P_e^T, \chi_e) \geqslant \gamma(\Omega, \mathcal{X}) \Rightarrow \dot{V}(\hat{P}_e^T, \hat{\chi}_e) < 0. \quad (13)$$

In other terms, $\mathcal{A}(\Omega, \mathcal{X})$ is defined as a contour surface of V, outside which the Lyapunov function decreases when estimated values are considered. The shape and the size of the domain $\mathcal{A}(\Omega, \mathcal{X})$ determine the robustness property of the problem.

Several tracking and path-following controls have been proposed for mobile robots (Kanayama *et al.* 1991, Aït-Abderrahim 1991, Samson 1992, Canudas *et al.* 1994) in the nominal case, that is when the state variables are supposed to be exactly known. The proof of asymptotic stabilization of the proposed systems involves Lyapunov functions with negative semidefinite derivative, and the convergence is proven by means of La Salle's or Barbalat's theorem. In the case when estimated values are considered, it is no longer possible to use such complementary lemmas; a negative semidefinite function does not lead to a stability statement (Hamel *et al.* 1994). Hamel and Meizel (1996) proved the stability for a new controller by means of a Lyapunov function with negative definite derivative. In this case an algorithm, based on D–K iteration used in H_∞ control, is proposed for computing the attractive domain $\mathcal{A}(\Omega, \mathcal{X})$.

In this paper we propose a new control strategy, based on a combination of appropriate sliding surface with the use of a Lyapunov function allowing the attractive domain to be computed analytically.

3. Robust dynamic state feedback controller

In this section we design the path-following control by determining an appropriate sliding surface ($z_e = 0$), defined by:

$$z_e = y_e + \lambda \operatorname{sgn}(v_c)\, \theta_e + \mu \chi_e, \quad \lambda, \mu > 0. \quad (14)$$

We are going to prove, in the following, that the convergence of y_e, θ_e and χ_e to zero can be ensured once the state space is reduced to the surface $z_e = 0$. First, to guarantee the convergence of z_e to zero we impose the following dynamics on the variable z_e:

$$\dot{z}_e = -|v_c| \frac{k}{\lambda} z_e, \quad k > 0; \quad (15)$$

the control law u_c becomes

$$u_c = \dot{\chi}_r^r - \frac{|v_c|}{\mu} \left(\operatorname{sgn}(v_c) \sin \theta_e + \lambda \chi_e + \frac{k}{\lambda} z_e \right). \quad (16)$$

3.1. *Stability*

Now, with the aim of proving the stability of the origin of the state space for system (7) under control (16), we introduce the following Lyapunov function:

$$V(P_e^T, \chi_e) = \frac{\lambda}{2} \left[k z_e^2 + \lambda^2 \mu \chi_e^2 + 4\lambda^2 \sin^2 \left(\frac{\theta_e}{2} \right) \right]. \quad (17)$$

Using (7) and (16) the time derivative of V can be expressed as follows:

$$\dot{V}(P_e^T, \chi_e) = -|v_c|(k^2 z_e^2 + \lambda^2 k \chi_e z_e + \lambda^4 \chi_e^2). \quad (18)$$

As $\dot{V}(P_e^T, \chi_e)$ is a semidefinite negative function, and as the set of points $\{z_e = \chi_e = 0,\ y_e = -\lambda \operatorname{sgn}(v_c)\, \theta_e\}$ over which $\dot{V}$ vanishes (under the hypothesis that v_c does not converge to zero†) constitutes an invariant set for system (7), we know from La Salle's theorem that any trajectory starting from a well-defined bounded region will converge to this set. Furthermore, as

† $v_c = 0$ means that the dynamics of system (6) vanish and that the vehicle stops.

$y_e = -\lambda \operatorname{sgn}(v_c)\,\theta_e$ once $z_e = 0$, the dynamics of y_e given by (7) become

$$\dot{y}_e = -|v_c| \sin\left(\frac{y_e}{\lambda}\right).$$

Therefore, paths starting from the region where $z_e = \chi_e = 0$ and $|y_e| < \lambda\pi$ will converge to the origin point $x_e = y_e = \theta_e = \chi_e = 0$. Now, the remaining question that we need to answer is: how can we ensure that the representative point controlled by (16) will reach the manifold $z_e = \chi_e = 0$ within the region where $|y_e| < \lambda\pi$?

We can answer this question by considering the Lyapunov function (17). From figure (4), where several contour surfaces of V are represented, it appears that there exists a value V^0 (one can verify easily that $V^0 = 2\lambda^3$; this value is obtained for $z_e = 0$, $\chi_e = 0$ and $\theta_e = (2n+1)\pi$) such that the set of point (P_e^T, χ_e) verifying $V(P_e^T, \chi_e) \leqslant V^0$ is the infinite union of compacts sets connected to one another by a unique point on the θ axis. Therefore, the domain

$$\mathcal{S} = \{(P_e^T, \chi_e)/V(P_e^T, \chi_e) < V^0, \\ \theta_e \in (-\pi, \pi), 1 - \chi_r y_e > 0\}$$

defines an open neighbourhood of the origin point $(P_e^T = 0, \chi_e = 0)$. Now, as V is a decreasing function of the state, if a trajectory starts inside the domain $\mathcal{S}$, the representative point converges to the unique equilibrium point $(P_e = 0, \chi_e = 0)$. Note that, depending on the initial conditions, the gains λ, μ and k can be chosen such that the initial point belongs to $\mathcal{S}$, ensuring the convergence of the corresponding trajectory to zero. A practical computation of the set $\mathcal{S}$ can be obtained following the same method as developed by Hamel and Meizel (1996); this is done in appendix A.

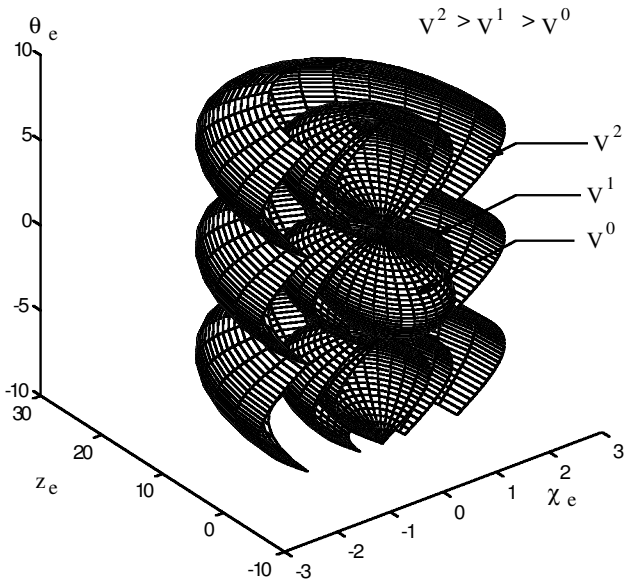

Figure 4. Domain of stability.

3.2. *Control robustness*

Let us go back to system (7) and consider the closed-loop control (9) with the estimated state values instead of the exact values. We obtain

$$\begin{pmatrix} \dot{y}_e \\ \dot{\theta}_e \\ \dot{\chi}_e \end{pmatrix} = \begin{pmatrix} v_c \sin\theta_e \\ v_c \chi_e \\ u_c(\hat{P}_e^T, \hat{\chi}_e) - \dot{\chi}_r^r \end{pmatrix}, \tag{19}$$

with

$$u_c(\hat{P}_e^T, \hat{\chi}_e) = \dot{\hat{\chi}}_r^r - \frac{|v_c|}{\mu}\left(\operatorname{sgn}(v_c) \sin\hat{\theta}_e + \lambda\hat{\chi}_e + \frac{k}{\lambda}\hat{z}_e\right) \tag{20}$$

and $\hat{\theta}_e = \theta_e + \delta\theta_e$, $\hat{\chi}_e = \chi_e + \delta\chi_e$, $z_e = z_e + \delta z_e$ and $\dot{\hat{\chi}}_r^r = \dot{\chi}_r^r + \delta\dot{\chi}_r^r$. Under the hypothesis that the error $\delta\theta_e$ is small enough, we consider the following first-order approximation: $\sin\hat{\theta}_e \approx \sin\theta_e + \delta\theta_e \cos\theta_e$.

Replacing this expression in (20), we obtain

$$\dot{\chi}_e = -\frac{|v_c|}{\mu}\left(\operatorname{sgn}(v_c) \sin\theta_e + \lambda\chi_e + \frac{k}{\lambda} z_e + \epsilon\right), \tag{21}$$

where ϵ represents the error term:

$$\epsilon = \operatorname{sgn}(v_c)\,\delta\theta_e \cos\theta_e + \lambda\,\delta\chi_e \\ + \frac{k}{\lambda}(\delta y_e + \lambda \operatorname{sgn}(v_c)\,\delta\theta_e + \mu\,\delta\chi_e) - \frac{\mu}{|v_c|}\delta\dot{\chi}_r^r. \tag{22}$$

Using the estimated values, the dynamics of z_e (given by (15) in the nominal case) turn out to be

$$\dot{z}_e = -|v_c|\left(\frac{k}{\lambda} z_e + \epsilon\right). \tag{23}$$

Now, in order to prove that the representative point converges towards an attractive domain let us consider the Lyapunov function (17) anew and compute its time derivative with respect to the dynamics of system (19):

$$\dot{V} = -\frac{|v_c|}{2}(k^2 z_e^2 + k\lambda z_e\epsilon + \lambda^4\chi_e^2 + \lambda^2 k z_e\chi_e + \lambda^3\chi_e\epsilon) \\ = -\frac{|v_c|}{2}(X^T\Sigma X - H),$$

where

$$X = (z_e + \lambda\epsilon/3k, \lambda\chi_e + \epsilon/3),$$

$$\Sigma = \begin{pmatrix} k^2 & \frac{\lambda k}{2} \\ \frac{\lambda k}{2} & \lambda^2 \end{pmatrix}$$

and $H = \lambda^2\epsilon^2/3$.

3.2.1. *Computation of the attractive domain* $\mathcal{A}(\Omega, \mathcal{X})$. From this last expression, the set of points verifying $\dot{V} = 0$ may be viewed as the contour curve corresponding to the value H for the Riemannian distance defined by the definite positive matrix Σ in the (z_e, χ_e) plane, with respect to the new frame centred at $(-\lambda\epsilon/3k, -\epsilon/3)$ and whose basis is obtained by keeping the same unit vector along the z_e axis and by multiplying by $1/\lambda$ the unit vector along the χ_e axis. Depending on the sign of ϵ, the set of points verifying $\dot{V} = 0$ is defined by two symmetric ellipses with respect to the origin (figure 5). From this representation we know that $\dot{V} < 0$ for $X^T \Sigma X > H$, that is outside the contour curve $\dot{V} = 0$.

Using Lagrange multipliers we can simply compute the extremal values of z_e and χ_e along the contour curve $\dot{V} = 0$. Considering the augmented function $G_{z_e} = z_e + m\dot{V}$, $m \in \mathbb{R}$ and writing that $\partial G_{z_e}/\partial \chi_e = \partial G_{z_e}/\partial z_e = 0$, we deduce that extremal values of z_e are obtained for $\chi_e = -(kz_e + \lambda\epsilon)/2\lambda^2$. Replacing this last expression in equation $\dot{V} = 0$, we obtain

$$-\frac{\lambda\epsilon}{k} \leqslant z_e \leqslant \frac{\lambda\epsilon}{3k} \quad \text{when } \epsilon > 0,$$
$$\frac{\lambda\epsilon}{3k} \leqslant z_e \leqslant -\frac{\lambda\epsilon}{k} \quad \text{when } \epsilon < 0.$$

Note that $\chi_e = 0$ when $z_e = -\lambda\epsilon/k$ and $\chi_e = -2\epsilon/3\lambda$ when $z_e = \lambda\epsilon/3k$.

Using the same reasoning with the augmented function $G_{\chi_e} = \chi_e + m\dot{V}$, $m \in \mathbb{R}$ we obtain

$$-\frac{\epsilon}{\lambda} \leqslant \chi_e \leqslant \frac{\epsilon}{\lambda} \quad \text{when } \epsilon < 0,$$
$$\frac{\epsilon}{3\lambda} \leqslant z_e \leqslant -\frac{\epsilon}{\lambda} \quad \text{when } \epsilon > 0.$$

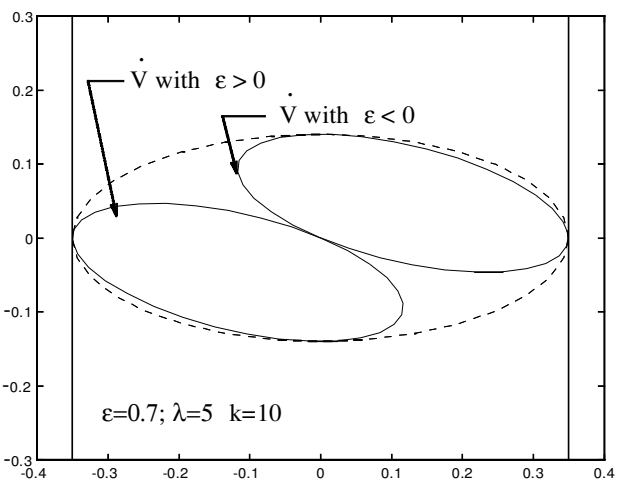

Figure 5. The attractive domain in the (z_e, χ_e) plane.

$z_e = 0$ when $\chi_e = -\epsilon/\lambda$, and $z_e = -\epsilon/3k$ when $\chi_e = \epsilon/\lambda$.

This construction characterizes the projection of the equipotential curve $\dot{V} = 0$ in the (z_e, χ_e) plane. Now, in order to compute the attractive set we need to determine the bounds for the other two state variables y_e and θ_e. To compute these bounds more easily we are going to consider a convex hull of the two ellipsoids obtained for $\epsilon > 0$ and $\epsilon < 0$. Let us consider the ellipse centred at the origin $(z_e = 0, \chi_e = 0)$, whose equation is given by:

$$\frac{1}{\lambda^2} z_e^2 + \frac{\lambda^2}{k^2} \chi_e^2 = \frac{\epsilon^2}{k^2}. \tag{24}$$

This ellipse is tangent to the previous two ellipses ($\epsilon > 0$ or $\epsilon < 0$): vertically at the points $(z_e = \lambda\epsilon/3k, \chi_e = 0)$ and horizontally at the points $(z_e = 0, \chi_e = -\epsilon/\lambda)$. It is the smallest ellipse centred at the origin, with vertical and horizontal axes and containing the two ellipses. Therefore, it constitutes a good approximation of their union (see figure 5). From this approximation, we can now easily determine bounds on the remaining two state variables as follows. As $z_e = y_e + \lambda\theta_e \operatorname{sgn}(v_c) + \mu\chi_e$,

$$\theta_e = -\frac{y_e - (z_e - \mu\chi_e)}{\lambda} \operatorname{sgn}(v_c). \tag{25}$$

Therefore the dynamics of y_e given by (19) become

$$\dot{y}_e = -|v_c| \sin\left(\frac{y_e - (z_e - \mu\chi_e)}{\lambda}\right) \tag{26}$$

and then, so long as $|y_e| < |z_e - \mu\chi_e|$, $|y_e|$ decreases.

To compute a bound for y_e let us look for the maximum value of $z_e - \mu\chi_e$ over the ellipse (24). Once more we use Lagrange multipliers. Consider the augmented function

$$G_{(z_e - \mu\chi_e)} = z_e - \mu\chi_e + m(z_e^2/\lambda^2 + \lambda^2\chi_e^2/k^2 - \epsilon^2/k^2).$$

Writing that $\partial G_{(z_e - \mu\chi_e)}/\partial z_e = \partial G_{(z_e - \mu\chi_e)}/\partial \chi = 0$, we obtain $\chi_e = -\mu k^2 z_e/\lambda^4$; replacing this expression in (24) gives

$$z_e = \pm\frac{\lambda^3\epsilon}{k(\lambda^4 + \mu^2k^2)^{1/2}} \quad \chi = \pm\frac{\epsilon\mu k}{\lambda(\lambda^4 + \mu^2k^2)^{1/2}}. \tag{27}$$

The maximum value of $|z_e - \mu\chi_e|$ is then obtained when the signs of z_e and χ_e are opposite:

$$\max|z_e - \mu\chi_e| = \frac{|\epsilon|(\lambda^4 + \mu k^2)}{k\lambda(\lambda^4 + \mu^2k^2)} = Y. \tag{28}$$

Therefore, so long as $|y_e| > Y$, $|y_e|$ decreases.

Now, as $\theta_e = (z_e - \mu\chi_e - y_e)/\lambda$ the bound on θ_e can be deduced as follows:

$$|\theta_e| \leqslant \frac{2Y}{\lambda} = \Theta. \tag{29}$$

This last bound achieves the characterization of the domain of attraction as the set of points (χ_e, y_e, θ_e) in $\mathbb{R}^3$ defined by

$$\mathcal{A}_1(\Omega,\mathcal{X}) = \left\{ (y_e,\theta_e,\chi_e) \in [-Y,\, Y]\times[-\Theta,\Theta]\times\left[-\frac{\epsilon}{\lambda},\frac{\epsilon}{\lambda}\right], \right.$$
$$\left. \text{such that} \quad \frac{z_e^2}{\lambda^2}+\frac{\lambda^2\chi_e^2}{k^2}-\frac{\epsilon^2}{k^2}\leqslant 0 \right\}.$$

If we want to determine the attractive domain $\mathcal{A}(\Omega,\mathcal{X})$ by means of the definition stated in § 2.3, we have to consider the smallest equipotential of V surrounding the cylinder $\mathcal{A}_1(\Omega,\mathcal{X})$. It must be noticed that this latter definition of $\mathcal{A}(\Omega,\mathcal{X})$ provides a pessimistic representation of the actual attractive domain (figure 6).

3.2.2. *Interesting features of the result*. The precision specification is of great utility to design collision free path following processes when the closed-loop control is performed with estimated values. In other terms, if we assume the inaccuracy domains Ω and $\mathcal{X}$ to be known *a priori,* the path following process is said to be achievable if, for any configuration taken on the perturbed path with control precision $\mathcal{A}_1(\Omega,\mathcal{X})$, the vehicle does not intersect any obstacle. From the maximal bound Y on y_e, we determine a bound along the reference path where the representative point could lie during the path following process. Then, considering the actual robot shape and the maximal bound Θ on θ_e, we can deduce directly a security margin to avoid obstacles. Figure 7(a), presents a real situation (a vehicle in a corridor). The uncertain localization set Ω considered here is a truncated cylinder (half-height $\delta\theta_c = 0.05\,\text{rad}$ and radius $\delta x_c(\delta y_c) = 0.15\,\text{m}$) centred around the estimated configuration (we have fixed $\mathcal{X} = [-0.01\,\text{m}^{-1}, 0.01\,\text{m}^{-1}]$). One notices that, along the line segment, the vehicle may collide with obstacles because the projection of $\mathcal{A}_1(\Omega,\mathcal{X})$ on the (y_e,θ_e) plane is given by $Y = 0.9\,\text{m}$ and $\Theta = 0.36\,\text{rad}$ (see figure 7(*b*)). In this case, the planned path through the corridor does not appear to be safe. Changing the values of the controller gains (see figure 7(*c*)) the robot trajectory does not collide with obstacles any longer (the projection of $\mathcal{A}_1(\Omega,\mathcal{X})$ on the (y_e,θ_e) plane is given by $Y = 0.27\,\text{m}$ and $\Theta = 0.08\,\text{rad}$).

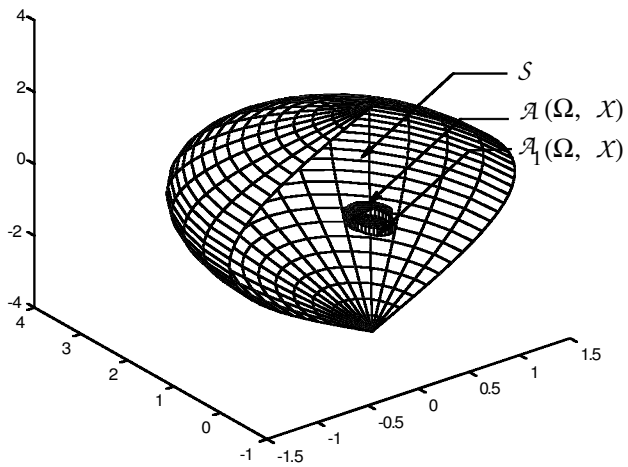

Figure 6. The attractive domain in $\mathcal{A}_1(\Omega,\chi)$.

In conclusion, if one wants the vehicle to achieve a mission safely, the size of the attractive domain $\mathcal{A}_1(\Omega,\mathcal{X})$ (or $\mathcal{A}(\Omega,\mathcal{X})$) has to be minimized under the constraint that a judicious balance between response time, no output oscillation and the size of the stability domain $\mathcal{S}$ has to be found. Under these constraints, it is not an easy task to find a compromise between the different parameters. We are going to show in the next section that the problem can be simplified if we introduce a discontinuity in the closed-loop control to design a variable structure control.

3.2.3. *Variable structure control.* We are going to prove that the new control $\tilde{u}_c$ defined by†

$$\tilde{u}_c(\hat{P}_e,\hat{\chi}_e) = u_c(\hat{P}_e,\hat{\chi}_e) - \frac{|v_c|}{\mu}[\epsilon+\beta\,\text{sgn}\,(\hat{z}_e)] \tag{31}$$

ensures the convergence of the system towards an attractive domain $\mathcal{A}(\Omega,\mathcal{X})$, under the hypotheses that the error $\delta\theta_e$ is small enough ($\sin\hat{\theta}_e \approx \sin\theta_e + \delta\theta_e\cos\theta_e$), and that β verifies

$$\beta > \epsilon_m,$$

where ϵ_m represents the maximal bound of ϵ on $(\Omega,\mathcal{X})$.

First, we prove the asymptotic convergence of the sliding variable z_e defined by (14) towards a compact neighbourhood of zero, defined by

$$I_m = [-\delta_m z_e, \delta_m z_e], \quad \text{with}\ \delta_m z_e = \delta_m y_e + \lambda\,\delta_m\theta_e + \mu\,\delta_m\chi_e, \tag{32}$$

where $\delta_m y_e$, $\delta_m\theta_e$ and $\delta_m\chi_e$ represent the maximal bounds on δy_e, $\delta\theta_e$ and $\delta\chi_e$, respectively which are supposed to be known *a priori*. Afterwards, we describe the attractive domain for the state variables using the bounds $\delta_m y_e$, $\delta_m\theta_e$, $\delta_m\chi_e$ and $\delta_m z_e$. Replacing the expression for $\tilde{u}_c$ given by (31) in (7) we obtain

$$\dot{\chi}_e = -\frac{|v_c|}{\mu}\left(\text{sgn}\,(v_c)\,\sin\theta_e + \lambda\chi_e + \frac{k}{\lambda}z_e + \epsilon + \beta\,\text{sgn}(\hat{z}_e)\right) \tag{33}$$

where ϵ is defined by (22). The derivative of z_e is

† In the nominal case ($\epsilon_m = 0$), taking $\beta = 0$, $\tilde{u}_c$ and u_c are identical.

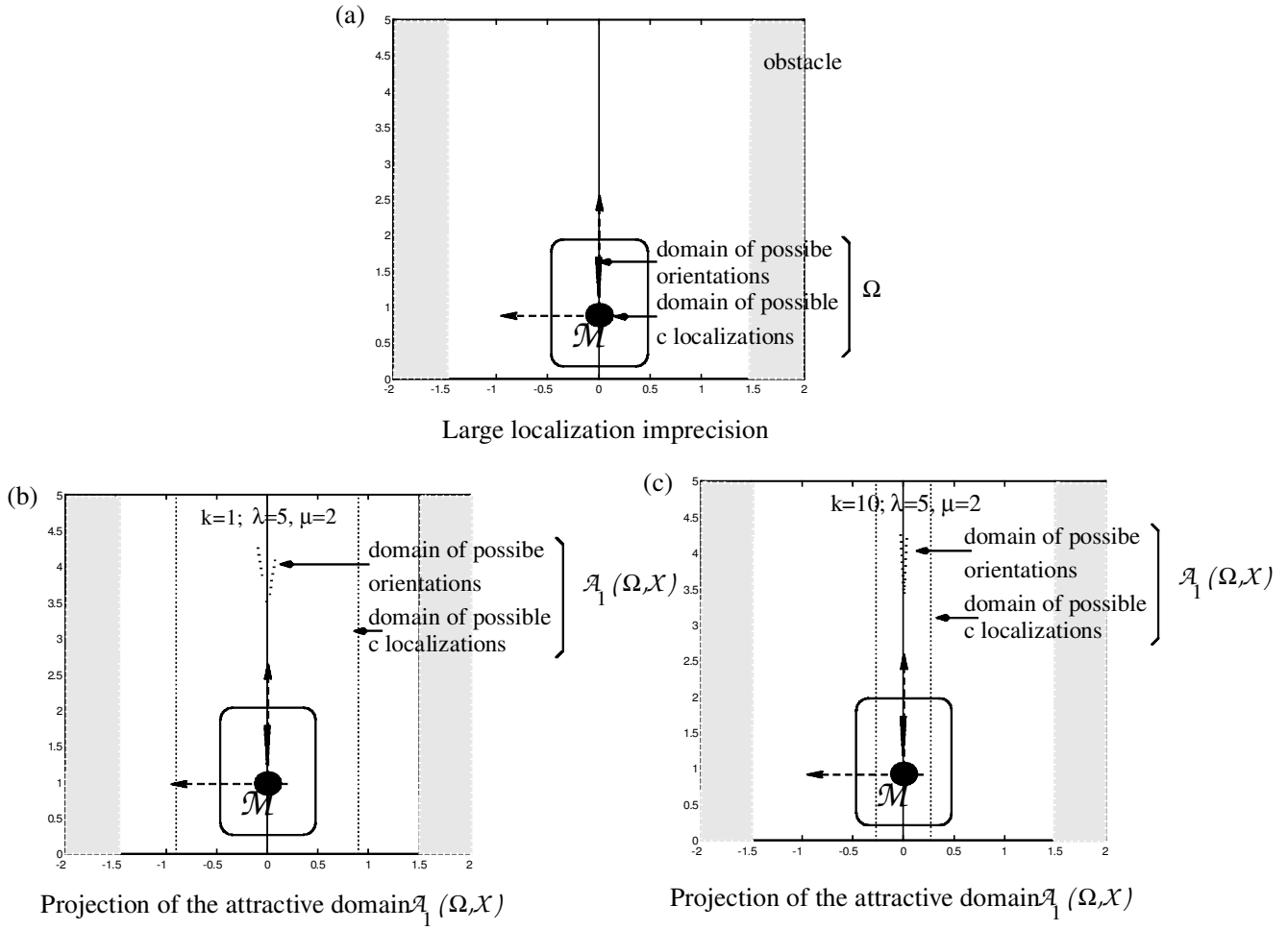

Figure 7. Projection of $\mathcal{A}_1(\Omega,\chi)$ along the planned path.

$$\dot{z}_e = -|v_c|\left(\frac{k}{\lambda} z_e + \epsilon + \beta \operatorname{sgn}(\hat{z}_e)\right). \tag{34}$$

Depending on the sign of δz_e, let us describe the behaviour of z_e. Suppose that $\hat{z}_e > 0$ $(z_e > -\delta z_e)$, $\dot{z}_e$ can be written in the following form:

$$\dot{z}_e = -\frac{k}{\lambda}|v_c|(z_e + H_1),$$

with

$$H_1 = \frac{\lambda}{k}(\beta + \epsilon) \geqslant 0.$$

Consequently, z_e converges towards $-H_1$ exponentially. In the same manner, when $\hat{z}_e < 0$ $(z_e < -\delta z_e)$, $\dot{z}_e$ can be written as

$$\dot{z}_e = -\frac{k}{\lambda}|v_c|(z_e - H_2),$$

with

$$H_2 = \frac{\lambda}{k}(\beta - \epsilon) \geqslant 0,$$

so that z_e converges towards H_2 exponentially, as well. Without lost of generality, we analyse the case when $H_1 > |\delta z_e|$, and $H_2 > |\delta z_e|$. The variation in z_e is shown in figures (8) and (9); we can see that z_e converges to $[-|\delta z_e|, |\delta z_e|] \subset [-\delta_m z_e, \delta_m z_e]$. Now, when $H_1 \leqslant |\delta z_e|$ or $H_2 \leqslant |\delta z_e|$, z_e goes towards an interval which is included in the previous attractive domain. Figure

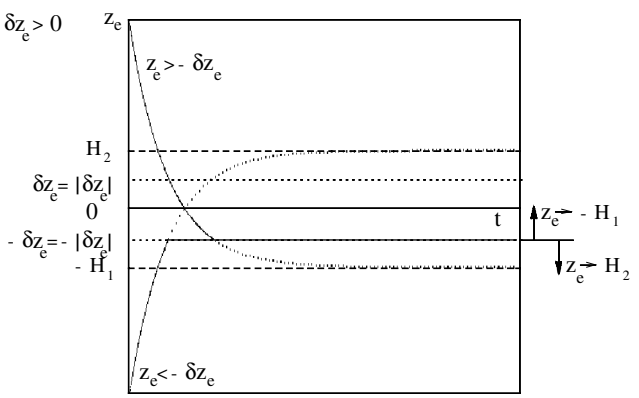

Figure 8. Variation in z_e when $\delta z_e > 0$.

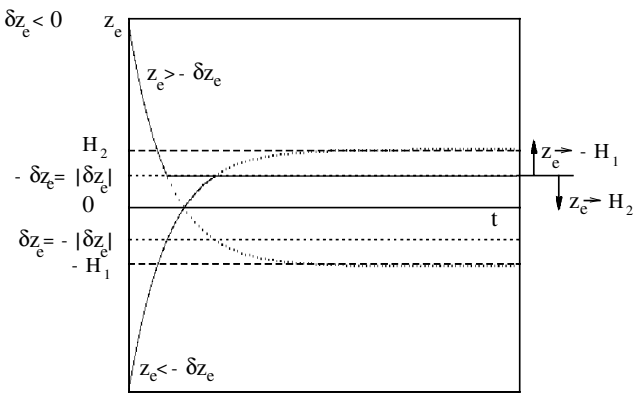

Figure 9. Variation in z_e when $\delta z_e < 0$.

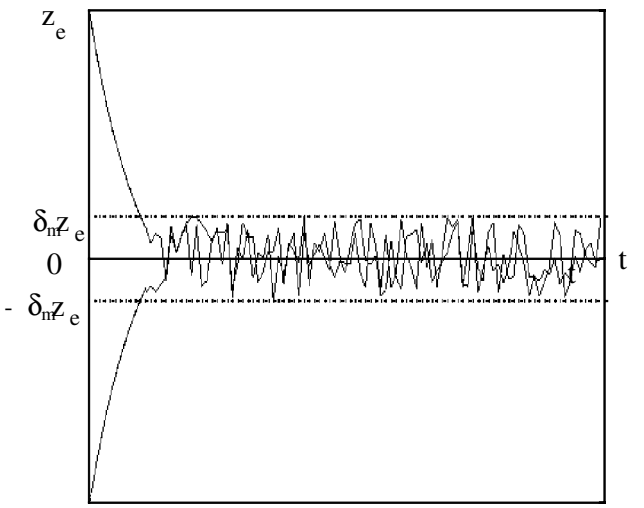

Figure 10. Behaviour of z_e when δz_e is time varying.

(10), represents the behaviour of z_e in the more realistic case when δz_e is a time-varying function. Another way to analyse the convergence of z_e consists in defining the interval of z_e in which the sliding condition $z_e \dot{z}_e < 0$ is verified†. At this stage, we ensure that z_e converges to I_m (32) exponentially. Now, we want to determine an attractive domain for all the state variables. Considering the Lyapunov function (17) with the estimated values we can prove, using the same reasoning as before (§ 3.2.1), that the state variables belong to a bounded compact region of the state space delimited at each time by the equipotential surface. From this, we know that the system variables do not diverge during the transition phase. Around each point of the reference path, we want to characterize an attractive domain around the origin where the representative points could possibly lie when z_e has reached I_m. First, we are going to determine a bound on the state variable χ_e by using a new Lyapunov function V_2 (deduced from V_1); from these values and the bound on z_e, we shall finally deduce bounds for y_e and θ_e. Let us consider the following non-negative function:

$$V_2 = \frac{1}{2}\left[\mu\chi_e^2 + 4\,\sin^2\left(\frac{\theta_e}{2}\right)\right]. \tag{35}$$

Its time derivative is

$$\dot{V}_2 = -\chi_e|v_c|\left(\lambda\chi_e + \frac{k}{\lambda z_e + \epsilon}\right).$$

As a scalar function of χ_e, this is the expression of a downward-oriented parabola, which crosses the χ_e axis when $\chi_e = 0$ and $\chi_e = -(1/\lambda)[\epsilon + (k/\lambda)z_e + \beta\,\mathrm{sgn}\,(\hat{z}_e)]$. So that, outside these values, $\dot{V}_2 < 0$, ensuring the convergence of χ_e to this interval. Using the previous maximation, we have

$$\chi_e \longrightarrow [-\chi_{e_m}, \chi_{e_m}],$$

with

$$\chi_{e_m} = \frac{1}{\lambda}(\epsilon_m + \frac{k}{\lambda}\,\delta_m z_e + \beta).$$

Remark 2: According to the definition of V_1, a condition for χ_e to stay within the stability domain is that β belongs to $[\epsilon_m, \lambda\,\chi_{e_m} - \epsilon_m - k\,\delta_m z_e]$. Choosing a large value for β induces a low chattering on z, however as a consequence the bound χ_{em} is higher and the curvature inaccuracy is increased. Note that χ_{e_m} can be also modified by regulating λ. It appears then important to find the balance between both constraints in tuning the gains. □

Pursuing in the same way as in § 3.2.1, the bound on y_e can be given by computing the maximum of $z_e - \mu\chi_e$ for $z_e \in [-\delta_m z_e, \delta_m z_e]$ and $\chi_e \in [-\chi_{e_m}, \chi_{e_m}]$.

$$\max|z_e - \mu\chi_e| = \delta_m z_e\left(1 + \frac{k\mu}{\lambda^2}\right) + \frac{\mu}{\lambda}\,(\epsilon_m + \beta) = Y. \tag{36}$$

Therefore, so long as $|y_e| > Y$, $|y_e|$ decreases. As $\theta_e = (z_e - \mu\chi_e - y_e)/\lambda$, the bound on θ_e can be deduced as follows:

$$|\theta_e| \leqslant \frac{2Y}{\lambda} = \Theta. \tag{37}$$

Now let us compare the new expression for the bound Y on y_e given by (36) with the expression given by (28). According to (28), if λ increases, the initial bound Y also increases. Therefore, it was not possible to enlarge the size of the stability domain by increasing λ, without enlarging the size of the attractive domain at the same time. Using the new bound Y given by (36) it appears that Y decreases when λ increases, and therefore the

† This condition ensures the convergence of z_e to 0.

balance between the different gains can be obtained easily.

4. Experimental results

The proposed controller has been implemented on a ROBUTER^{TM} (figure 11) using the Vx-Works real-time kernel. Three classes of experiments are shown in the following. Each class presents two experiments obtained with and without variable structure control respectively, for a specific choice of the controller gains k. We have set $\lambda = 5$, $\mu = 2$, for all the experiments and the variable structure controls are defined with $\beta = 5$. In each case the vehicle has to follow a reference path 9 m long, successively made up with a line segment, three arcs of circle and a final line segment (figure 12). The minimal distance between this path and the obstacles is 0.6 m. This trajectory represents the output of a typical path planner. Initial configuration and curvature errors are $(\hat{P}_e^T(0), \hat{\chi}_e(0)) \approx (0, 2\,\text{cm}, \pi/6\,\text{rad}, 0)$.

Figure 11. The ROMO Sapiens robot.

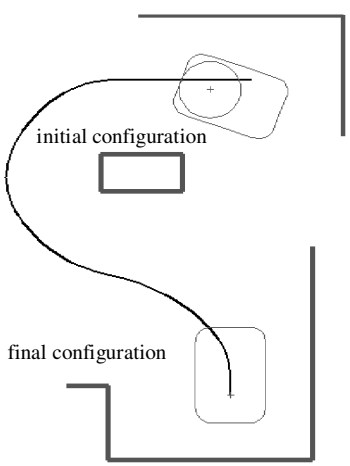

Figure 12. 'Experimental result'. The planned path for the ROBUTER^{TM}.

During these experiments, a constant speed of $20\,\text{cm}\,\text{s}^{-1}$ was maintained for the vehicle along the path. The sampling time T_e of the controller was fixed to 0.6 s. During T_e the mobile robot localization is continuously updated by integrating the wheels' rotation angle (odometry) and, when available, by exteroceptive (telemetric) measurements. They are processed by extended Kalman filtering and yield a configuration and a realized path curvature estimations $(\hat{P}_c^T, \hat{\chi}_c)$ with inaccuracies characterization $(\Omega, \mathcal{X})$.

Results are shown in figure 13; the experiments presented on the right and on the left have been obtained with and without sliding mode control techniques respectively. The boxes represent the configuration estimation of the vehicle, the ellipses represent the confidence domain of the position estimations; the obstacles are represented by thick lines.

The first class of experiment (figure 13(a)) has been obtained for $k = 1$. In this case it is not possible to ensure the existence of a security margin smaller than 0.6 m from the computation of $\mathcal{A}_1(\Omega, \mathcal{X})$. Using the first controller (without a sliding mode) the robot collides with the wall, while the stabilization is better with variable structure control ($\beta = 5$).

The classes of experiments in figures 13(b) and (c) have been obtained for $k = 3$ and $k = 10$ respectively. For these last two cases, it is possible to deduce from the computation of $\mathcal{A}_1(\Omega, \mathcal{X})$ the existence of a security margin smaller than 0.6 m. In both cases the path-following process is safe in accordance with the theoretical robustness result. Here again, one can see that the stabilization process is performed better when variable structure control is used. As we can see in figure 13, the chattering phenomenon does not appear. This is due, on the one hand, to the existence of the integrator, $(\dot{\chi}_e = u)$ that smooths the discontinuities and, on the other hand, to the sufficiently large value of β which induces a low switching frequency on z. However, an important drawback of discontinuous control is that the determination of β requires much attention, as mentioned in remark 2. Furthermore, β must be chosen small enough to avoid strong discontinuities in the control.

5. Conclusion

The method presented in this paper allows us to answer fully the question considered. It leads to the analytical characterization of an attractive domain around the equilibrium point which can be simply used to determine a security margin for avoiding obstacles during the path-following process. Although the use of a Lyapunov

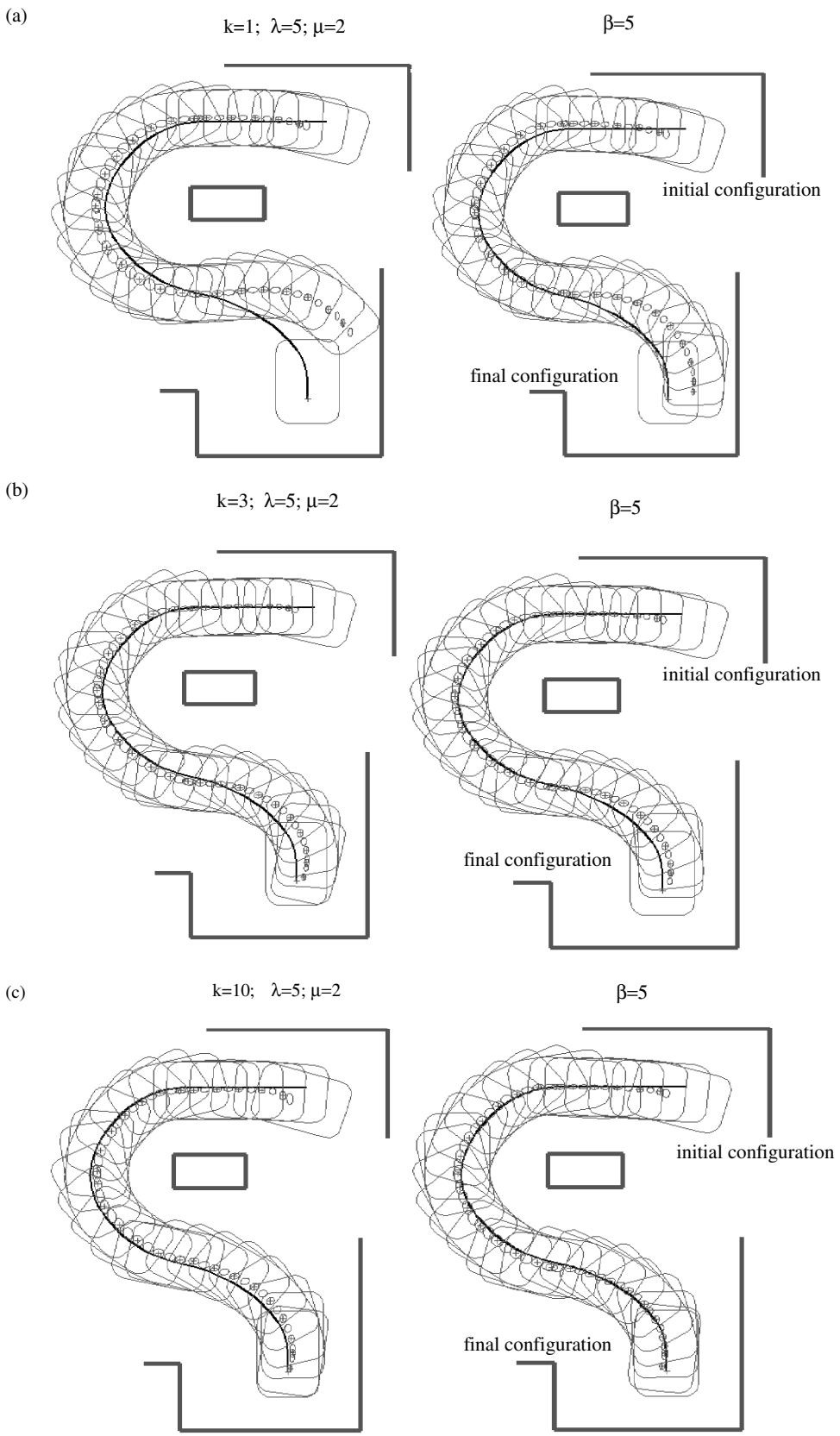

Figure 13. 'Experimental results'. The realized path for the ROBUTER^{TM}; each class of experiment has been obtained with (right) and without (left) variable structure control.

function to characterize the regulation precision generally provides an imprecise upper bound of the actual attractive domain, it appears here, through the experimental results, that the $\mathcal{A}_1(\Omega, \mathcal{X})$ domain characterizes the control robustness quite well. On the other hand, we have seen that the size of $\mathcal{A}_1(\Omega, \mathcal{X})$ can be reduced while keeping the balance between short response time, low output oscillations and large stability domain. This analysis is richer than a simple study of estimation error propagation which allows us to determine only safe motion in open loop. To our knowledge, at this time, no similar results exist involving other control techniques. It would be interesting, however, to compare the result of our approach with that obtained by other methods, and in particular H_∞-type robustness analysis performed on a linearized system.

Appendix A: Computation of the stability domain $\mathcal{S}$

Considering the definition given in § 3.1, it appears that the computation of the convergence domain $\mathcal{S}$, as defined, is not an easy task in practice. However, if we consider $|y_e| < 1/\chi_{r_m}$, ($\chi_{r_m} \triangleq 1/\rho_{\min}$) and assuming that

$$\forall (y_e, \theta_e, \chi_e) \in \mathbb{R} \times (-\pi,\ \pi) \times \mathbb{R},$$

$$V(P_e(0), \chi_e(0)) < \min\left(2\lambda^3, \frac{1}{2}\, k\lambda \frac{1}{\chi_{r_m}^2}\right),$$

then control (16) asymptotically stabilizes (y_e, θ_e, χ_e) at the origin. In the following we prove that the configuration and curvature errors converge to zero.

(*a*) The case when $2\lambda^3 < \frac{1}{2}k\lambda$ presents no problem.

(*b*) In the opposite case, we can easily show that z_{e_m}, the maximum of z_e on the contour curve $V(P_e, \chi_e) = V(P_e(0), \chi_e(0))$, is obtained for $\chi_e = \theta_e = 0$. Hence, $z_{e_m} = y_e$. However, as we want $|y_e|$ to remain lower than $1/\chi_{r_m}$, it suffices to take $V(P_e, \chi_e) < k\lambda/2\chi_{r_m}^2$.

Now let us analyse the relationship between initial conditions and controller gains. Let us take the simple case when $\mathcal{S} = \{(P_e, \chi_e)/V(P_e, \chi_e) < 2\lambda^3\}$ (we assume that $2\lambda^3 < k\lambda/2\chi_{r_m}^2$). In this case, the domain $\mathcal{S}$ must be bounded by $\theta_e = \pm\pi$. This leads us to find the relationship between the initial configuration error $(P_0^T, \chi_0) = (x_0, y_0, \theta_0, \chi_0)^T$ and the controller gains. Let

$$V_0 = \frac{\lambda}{2}\left[kz_0^2 + \lambda^2\mu\chi_0^2 + 4\lambda^2 \sin^2\left(\frac{\theta_0}{2}\right)\right] < 2\lambda^3. \quad \text{(A 1)}$$

Since $V(P_e, \chi_e)$ is decreasing in $\mathcal{S}$, it follows that

$$\frac{\lambda}{2}\left[kz_e^2 + \lambda^2\mu\chi_e^2 + 4\lambda^2 \sin^2\left(\frac{\theta_e}{2}\right)\right] < 2\lambda^3. \quad \text{(A 2)}$$

In order to assert that θ_{e_m}, the maximum of θ_e, is smaller than π, the inequality (A3) must be satisfied (v_c is assumed to be greater than zero):

$$\lambda^2[2(1 + \cos\ \theta_0 - k\theta_0^2 - \mu\chi_0^2] - 2k\theta_0(y_0 + \mu\chi_0)\lambda - k(y_0 + \mu\chi_0)^2 > 0. \quad \text{(A3)}$$

For example, if we consider $\chi_0 = 0$ and $2(1 + \cos\ \theta_0) - k\theta_0^2 > 0$, the inequality (A3) is satisfied if we choose λ greater than

$$k\theta_0 y_0\ + \frac{|y_0| \cos\,(\theta_0/2)(2k)^{1/2}}{[2(1 + \cos\ \theta_0) - k\theta_0^2]}.$$

Finally, for a given domain of possible initial conditions, we can always choose λ, k and μ such that the inequality be verified on the domain.

References

Canudas, C., Khennouf, H., Samson, C., and Sordalen, O. J., 1994. Nonlinear control design for mobile robots. *Mobile Robots,* edited by Y. F. Zheng (Singapore: World Scientific).

Cheesman, P., and Smith, R. C., 1986, On the representation and estimation of spatial uncertainty. *International Journal of Robotics Research* **5,** 56–68.

DeLuca, A., Oriolo, G., and Samson, C., 1997, Feedback control of a nonholonomic car-like robot. *Robot Motion Planning and Control,* Lecture Notes in Control and Information Sciences, Vol. 229, edited by J.-P. Laumond (Berlin: Springer-Verlag), pp. 171–253.

Durieu, C., Aldon, M. J., and Meizel, D., 1996, Multisensory data fusion for localisation in mobile robotics. *Traitement du Signal,* **13,** 143–165.

Hamel, T., Halbwachs, E., and Meizel, D., 1993, La Géometrie offre t-elle une alternative au filtrage de Kalman? *Localisation En Robotique, Proceedings of the SEE National Conference,* Supélec, Gif sur Yvette, France, 1993, pp. 53–61.

Hamel, T., and Meizel, D., 1996, Robust control laws for wheeled mobile robots. *Proceedings of the Triennial IFAC World Congress,* San Francisco, California, USA, 1996, [on CD-ROM].

Hamel, T., Meizel, D., and Charara, A., 1994, A new robust tracking controller for autonomous vehicles. *Proceedings of the Fourth IFAC Symposium on Robot Control,* Capri, Italy, 1994, pp. 93–99.

Kanayama, Y., Kimura, Y., Myazaki, F., and Noguchi, T., 1991, A stable tracking control method for an autonomous mobile robot. *Proceedings of the IEEE International Workshop on Intelligent Robots and Systems* (New York: IEEE), pp. 1236–1241.

Laumond, J.-P., Jacobs, P., Taïx, M., and Murray, R., 1994, A motion planner for nonholonomic mobile robots. *IEEE Transactions on Robotics and Automation*, pp. 577–593.

Leonard, J. J., and Durrant-Whyte, H., 1991, Mobile robot localization by tracking geometric beacons. *IEEE Transactions on Robotics and Automation,* **7,** 376–382.

Nelson, W. L., and Cox, I. J., 1988, Local path control for autonomous vehicle. *Proceedings of the IEEE International Conference on Robotics and Automation,* Philadelphia, Pennsylvania, USA, 1988 (New York: IEEE), pp. 1504–1510.

Preciado, A., Meizel, D., Segovia, A., and Rombaut, M., 1991, Fusion of multi-sensor data: a geometric approach. *Proceedings of the IEEE International Conference on Robotics and Automation* (New York: IEEE), pp. 2806–2811.

Sampei, M., Tamura, T., Itoh, T., and Nakamichi, M., 1991, Path tracking control of trailer-like mobile robot. *Proceedings of the*

IEEE International Workshop on Intelligent Robots and Systems, Osaka, Japan, 1991 (New York: IEEE), pp. 193–198.

SAMSON, C., 1992, Path following and time-varying feedback stabilization of a wheeled mobile robot. *Proceedings of the International Conference on ICARV,* Singapore, September 1992, pp. RO-13.1.1–RO-13.1.5.

SAMSON, C., and AÏT-ABDERRAHIM, K., 1991, Feedback control of a nonholonomic wheeled cart in cartesian space. *Proceedings of the IEEE International Conference on Robotics and Automation* (New York: 1EEE), pp. 1136–1141.

SIMÉON, T., and ALAMI, R., 1994, Planning robust motion strategies for a mobile robot in a polygonal world. *Revue d'Intelligence Artificielle,* **8,** 383–401.

SORDALEN, O. J., 1993, Feedback control of nonholonomic mobile robots. Technical Report 93-5-W, Department of Engineering Cybernetics, The Norwegen Institute of Technology.

SOUÈRES, P., and LAUMOND, J.-P., 1996, Shortest path synthesis for a car-like robot. *IEEE Transactions on Automatic Control,* **41,** 672–688.

THUILOT, B., 1994, Contribution à la modélisation et à la commande de robots mobiles à roues. PhD Thesis, Ecoles des Mines de Paris.

TOUNSI, M., LEBERT, G., and GAUTIER, M., 1995, Dynamic control of nonholonomic mobile robot in cartesian space. *Proceedings of the 34th IEEE Conference on Decision and Control,* New Orleans, Louisianna, USA, 1995 (New York: IEEE).